

Density profile and line-of-sight mass contamination of SLACS gravitational lenses

Antonio C. C. Guimarães and Laerte Sodré Jr.

*Departamento de Astronomia, Universidade de São Paulo,
Rua do Matão 1226, CEP 05508-090 São Paulo - SP, Brazil*

aguimaraes@astro.iag.usp.br

ABSTRACT

We use data from 58 strong lensing events surveyed by the Sloan Lens ACS Survey to estimate the projected galaxy mass inside their Einstein radii by two independent methods: stellar dynamics and strong gravitational lensing. Four models are examined testing the galaxy-lens density profile and a possible line-of-sight (l.o.s.) mass contamination. We test a fixed isothermal profile and a power-law with free index, both without and with contamination. For each model, a likelihood analysis is performed to find the parameters that produce the best agreement between the dynamical and lensing masses, and the parameters confidence levels. The Bayesian evidence is calculated to allow a comparison among the models.

We find that there is evidence for a l.o.s. mass contamination of the order of 10%, and that the preferred density profile is close to an isothermal profile, $\rho \propto r^{-2}$. If the l.o.s. contamination is neglected, the density profile determined by a joint lensing and dynamical analysis is flatter than isothermal.

Subject headings: dark matter — galaxies: elliptical and lenticular, cD — galaxies: kinematics and dynamics — galaxies: structure — galaxies: fundamental parameters — gravitational lensing

1. Introduction

The observation of strong gravitational lensing events has allowed many studies about the mass, density profile and structure of the galaxies that act as lenses (Bolton et al. 2006; Treu et al. 2006; Koopmans et al. 2006; Gavazzi et al. 2007; Bolton et al. 2007, 2008a,b; Czoske et al. 2008; Treu et al. 2008), which could also have important implications for dark matter and cosmology studies. Therefore it is fundamental to control for possible systematic effects, such as line-of-sight (l.o.s.) mass contamination. However most of these works consider a free path from source to lens and from lens to observer, even though there are observational and theoretical suggestions that the l.o.s. mass contamination may be significant.

Bar-Kana (1996) investigated theoretically the effect of the Large-Scale Structure on strong lensing events, finding that it can be significant.

Keeton et al. (1997) observed that external shear due to galaxies and clusters associated with the primary lens or along the l.o.s. can be an important perturbation in individual lens models. Premadi & Martel (2004) used ray-tracing to investigate the effect of density inhomogeneities along the l.o.s. of strong lenses and concluded that it can be of order 10% on the magnification of the sources. Dalal et al. (2005) found that significant errors can arise from l.o.s. projections when using giant arcs generated by cluster strong lensing to constrain the cosmological parameters. Wambsganss et al. (2005) noted that secondary matter along the l.o.s. of strong lenses can lead in some circumstances to an overestimate of 10-15% of the primary lens mass if ignored. Using spectroscopy, Momcheva et al. (2006) and Williams et al. (2006) discovered a significant l.o.s. effect on strong lens galaxies. Moustakas et al. (2007) observed that even in

under-dense local environments, the l.o.s. contamination may give a considerable contribution to galaxy-scale strong lenses. Using ray-tracing thought the Millennium Simulation, Hilbert et al. (2007) determined that strong lensing lines-of-sight are biased towards higher than average mean densities, contributing a few percent to the total surface density, and Puchwein & Hilbert (2009) found that secondary matter along the l.o.s. has a large effect on the strong-lensing optical depth and the cross-section for cluster strong lensing. Treu et al. (2008) measured the over-density of galaxies around SLACS lenses and observed that typical contributions from external mass distributions are of order of few percent, but reaching 10-20% in some cases. Faure et al. (2008) considered strong and weak lensing observations in the COSMOS survey and compared with simulations, finding that strong lensed images with large angular separation were in the densest regions. On the other hand, Auger (2008) did not find an over-density of photometric sources along the l.o.s. of a limited sample of SLACS strong lenses in comparison with other SDSS massive early-type galaxies and interpreted that as evidence against a possible l.o.s. contamination.

In this paper we use two simple independent galaxy mass estimate methods, strong gravitational lensing and stellar dynamics, to examine the presence of l.o.s. mass contamination in the lens set. We use all the suitable events in the SLACS sample, considering a realistic brightness function for the lens-galaxies and taking into account seeing effects.

In Section 2 we describe how we calculate the mass of SLACS lenses using strong gravitational lensing and stellar dynamics, and how we determine the l.o.s. mass contamination. In Section 3 we show our results, which are discussed in Section 4, together with our conclusions.

2. Data and Methods

The analysis in this paper is based on the comparison of galaxy masses calculated through two different methods: gravitational lensing and dynamical analysis. In sec. 2.1 we present the data used in the analysis, collected from the SLACS survey.

In sections 2.2 and 2.3, we discuss the lens-

ing and dynamical mass determinations, respectively. We will assume simple models for the galaxy mass distribution (e.g., spherical symmetry, power-law density distribution) because they have few free parameters and allow to illustrate well the two methods. For a similar approach see Koopmans et al. (2006).

We want to examine whether the two mass estimates are indeed equivalent and/or if there is evidence of systematic differences between them. In particular, we consider the plausibility of a contamination affecting the lensing mass. Sec. 2.4 presents a Bayesian analysis of this problem.

2.1. Data

The selected set of galaxies is part of the Sloan Lens ACS Survey, SLACS (Bolton et al. 2006), which is a Hubble Space Telescope (HST) Snapshot imaging survey for strong gravitational galactic lenses. The candidates for the HST imaging were selected spectroscopically from the SDSS database and are a sub-sample of the SDSS Luminous Red Galaxy (LRG) sample.

We use data compiled from Koopmans et al. (2006), Gavazzi et al. (2007) and Bolton et al. (2008a), constructing a sample of 58 strong gravitational lensing events where the lenses are isolated early-type galaxies (E+S0). Data from SLACS is especially suitable for joint strong lensing and dynamical analysis because they allow precise determination of the Einstein radius for each lens-galaxy in a relatively homogeneous sample of early-type galaxies. And, at the same time, SDSS has precise stellar velocity dispersion measurements for the lenses, as well as redshifts of lenses and sources.

For each lens system we are interested in the redshift of the background lensed source z_s , the redshift of the lens z_l , the average stellar velocity dispersion inside an aperture σ_{ap} , the effective radius R_e and the Einstein radius θ_E . The sample average values for these quantities are $\langle z_l \rangle = 0.2$, $\langle z_s \rangle = 0.6$, $\langle \sigma_{ap} \rangle = 250 \text{ km s}^{-1}$, $\langle R_e \rangle = 2.2''$, and $\langle \theta_E \rangle = 1.2''$.

The source and lens redshifts were determined from the SDSS spectra, and the stellar velocity dispersion corresponds to the light-weighted average inside the $3''$ diameter SDSS fiber.

2.2. Lensing Mass

The estimated projected mass inside the Einstein radius $R_E = \theta_E D_L$, is given by

$$M_L = \frac{c^2}{4G} \frac{D_L D_S}{D_{LS}} \theta_E^2 , \quad (1)$$

where $D_{[L,S,LS]}$ is the angular-diameter distance of the lens, source, and between lens and source, respectively. These distances are calculated assuming a redshift-distance relation derived inside a chosen cosmological model that in the present paper is a concordance Λ CDM model with $\Omega_m = 0.3$, $\Omega_\Lambda = 0.7$ and $h = 0.7$.

The Einstein radii were determined from HST images using strong lensing modeling of the lenses and reconstruction of the unlensed sources (Koopmans et al. 2006; Gavazzi et al. 2007). The uncertainties on θ_E were reported to be around 5%, so we use this value for all Einstein radii. Note that the lensing modeling uses a Singular Isothermal Ellipsoid (SIE) mass model, but the resulting projected mass distribution is parameterized by an Einstein radius so that the enclosed mass in the projected ellipse is the same that would be enclosed in a projected circle from an equivalent Singular Isothermal Sphere. This is the radius we adopt here. Indeed, the Einstein radius determined this way is a robust attribute of the lens, being little sensitive to the lens model used [see Kochanek contribution in Meylan et al. (2006)].

2.3. Dynamical Mass

The dynamical mass is obtained through the Jeans equations (Binney & Tremaine 1987), which relates the gravitational potential to the stellar velocity dispersion. For a spherical halo and an isotropic velocity distribution, the radial stellar velocity dispersion is given by

$$\sigma^2(r) = \frac{1}{\nu} \int_r^\infty \nu \frac{\partial \Phi}{\partial r} dr . \quad (2)$$

The gradient of the gravitational potential can be written directly in terms of the mass density profile

$$\frac{\partial \Phi}{\partial r} = \frac{4\pi G}{r^2} \int_0^r \rho(r') r'^2 dr' , \quad (3)$$

and the luminosity distribution is approximated by a Hernquist (1990) profile

$$\nu(r) \propto \frac{1}{r^{\gamma_*} (r + r_*)^{4-\gamma_*}} , \quad (4)$$

where $\gamma_* = 1$ and $r_* = R_e/1.8153$ that, according to Koopmans et al. (2006), gives a good fit to the surface brightness profile of the galaxies in the sample.

We model the effect of seeing through a Gaussian smoothing of the galaxy projected luminosity. Therefore, the observed surface brightness profile is related to an intrinsic (no seeing) profile by

$$I_{obs}(\theta) = \frac{e^{-\theta^2/2\sigma_s^2}}{\sigma_s^2} \int_0^\infty I(\theta') I_0\left(\frac{\theta\theta'}{\sigma_s^2}\right) e^{-\theta'^2/2\sigma_s^2} \theta' d\theta' , \quad (5)$$

where I_0 is the modified Bessel function of first kind, and σ_s^2 is the Gaussian seeing variance. We use $\sigma_s = 0.64''$, which corresponds to a FWHM of 1.5''.

The seeing correction to the average velocity dispersion within the observational aperture is then given by

$$\frac{\sigma_{ap}^2}{(\sigma_{ap}^2)_{obs}} = \frac{\int_0^{\theta_{ap}} \sigma_p^2(\theta) I(\theta) \theta d\theta}{\int_0^{\theta_{ap}} [\sigma_p^2(\theta) I(\theta)]_{obs} \theta d\theta} \frac{\int_0^{\theta_{ap}} I_{obs}(\theta) \theta d\theta}{\int_0^{\theta_{ap}} I(\theta) \theta d\theta} , \quad (6)$$

where σ_p^2 is the projected velocity dispersion profile and $[\sigma_p^2(\theta) I(\theta)]_{obs}$ is defined in a way similar to $I_{obs}(\theta)$ in Eq.(5).

The luminosity-weighted average velocity dispersion within a given aperture is given by

$$\sigma_{ap}^2 = \langle \sigma_p^2(< R_{ap}) \rangle \equiv \frac{\int \nu \sigma^2 dV}{\int \nu dV} , \quad (7)$$

where the integration volume is an infinite cylinder of radius R_{ap} with axis along the l.o.s.

We adopt a profile of the form $\rho \propto r^\gamma$ for the total mass distribution and examine the case where the power-law index is a free parameter and the case of a fixed power $\gamma = -2$ (SIS, Singular Isothermal Sphere). In the former the dynamical mass has to be obtained numerically solving equations (2) and (7), but in the latter the dynamical mass within the Einstein radius R_E is simply

$$m_D^{SIS}(< R_E) = \frac{\pi}{G} \sigma_{ap}^2 R_E . \quad (8)$$

2.4. Statistical model

We want to compare the estimates of lensing and dynamical masses taking into account the possibility that masses obtained through gravitational lensing are affected by some type of contamination. Specifically, we consider a model where the real lensing mass m_L (assumed equal to the dynamical mass) is related to the measured lensing mass as

$$m_L = (1 - f_c)M_L, \quad (9)$$

where f_c gives the fractional mass contamination.

We shall consider four models. Our reference model (I0) is a SIS model ($\gamma = 2$) without contamination ($f_c = 0$). Model I1 is a SIS model allowing for contamination accordingly with Eq.(9). Models P0 and P1 are analogous to I0 and I1, but now γ is determined from a global fitting to the data.

For a given model, we assume that the likelihood that the lensing and dynamical masses of a certain galaxy are equal is

$$\mathcal{L}_i = \frac{1}{\sqrt{2\pi(\sigma_{L,i}^2 + \sigma_{D,i}^2)}} \exp \left[-\frac{(m_{L,i} - m_{D,i})^2}{2(\sigma_{L,i}^2 + \sigma_{D,i}^2)} \right], \quad (10)$$

and the joint likelihood for the whole set of N galaxies is given by

$$\mathcal{L} = \prod_{i=1}^N \mathcal{L}_i. \quad (11)$$

Free parameters are obtained through maximization of the joint likelihood.

To compare the four models we adopt the Bayesian evidence, defined as (Trotta 2007)

$$E \equiv \int \mathcal{L}(p)P(p)dp, \quad (12)$$

where $P(p)$ is the prior probability distribution in the parameter space p . We adopt a flat prior probability distribution for all the parameters considered: $f_c \in [0, 1]$ and $\gamma \in [-3, -1]$. The main appeal of this approach for model comparison is that the Bayesian evidence automatically implements Occam's razor by penalizing more strongly more complex models, those with more free parameters.

Barnabè & Koopmans (2007) also use a Bayesian framework to formulate a joint gravitational lensing and stellar dynamics analysis, but have a different approach than ours.

3. Results

We have analyzed the data described in sec. 2.1 with the four models I0, I1, P0 and P1. Table 1 summarizes the properties of each model, as well as the maximum likelihood estimates of the parameters γ and f_c (when appropriate). The table also shows the maximum likelihood and evidence of the models relative to our fiducial model I0, and the mean value of the ratio of the lensing to dynamical mass.

Figure 1 presents the likelihood function of models I1, P0 and P1, showing the best fit values for the free parameters as well as their confidence intervals. Figure 2 compares lensing and dynamical estimates for the four models with the parameters set at their maximum likelihood estimates.

Model I0 (SIS profile, no contamination) has no free parameters. An examination of the top-left panel of Figure 2 shows a trend, perceptible to the eye, for the lensing mass to be larger than the dynamical mass. The sample average of the mass ratio $\langle m_L/m_D \rangle$ is 1.14 ± 0.02 , where the individual ratios were weighted by the inverse of the errors and the reported uncertainty was propagated from the individual mass errors and divided by \sqrt{N} (deviation from the mean).

Model I1 has a SIS mass profile and one free parameter that accounts for a fractional mass contamination; its best value is $f_c = 0.11 \pm 0.02$. Model I1 has a higher maximum likelihood than model I0, what is expected since it has one free parameter more. But its Bayes evidence is also higher than model I0, essentially because it reduces significantly the discrepancy between the lensing and dynamical mass estimates. The gain in evidence from model I0 to model I1 is 12.8, what is qualitatively characterized (Trotta 2007) as strong evidence in favor of model I1 in relation to I0.

Model P0 has a free index in the power-law mass profile and no contamination. The best-fit model has a slope for the mass profile $\gamma \simeq -1.7$ (see Table 1), flatter than the SIS profile. How-

Table 1: Comparison among models and best parameters.

model	$\rho(r)$	l.o.s. cont.	$\Delta \ln \mathcal{L}_{max}$	$\Delta \ln E$	γ	f_c	$\langle m_L/m_D \rangle$
I0	$\propto r^{-2}$	no	0	0	-	-	1.14 ± 0.02
I1	$\propto r^{-2}$	yes	15.3	12.3	-	0.11 ± 0.02	1.01 ± 0.02
P0	$\propto r^\gamma$	no	8.2	5.6	-1.72 ± 0.06	-	1.10 ± 0.02
P1	$\propto r^\gamma$	yes	15.9	11.1	-2.07 ± 0.13	0.13 ± 0.03	1.01 ± 0.02

NOTE.—The first three columns inform the model name, the total matter density profile form, and if the model includes line-of-sight mass contamination or not, respectively. $\Delta \mathcal{L}_{max}$ and $\Delta \ln E$ are calculated in relation to the corresponding values for model I0 ($\ln \mathcal{L}_{max} = \ln E = 1479.3$). The last three columns give the best fit parameters, γ and f_c , and $\langle m_L/m_D \rangle$ is the sample average of the masses ratio for each model at the point of maximum likelihood.

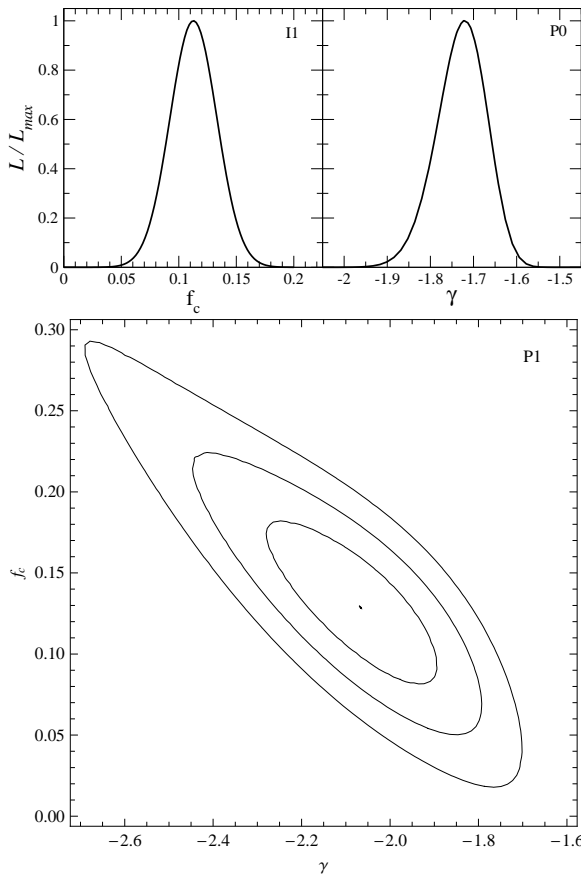


Fig. 1.— Likelihood analysis. The top panels show the likelihood functions for models I1 (left) and P0 (right). The bottom panel shows the likelihood contours for model P1, corresponding to the 1σ , 2σ and 3σ confidence levels, from the maximum likelihood point out, respectively.

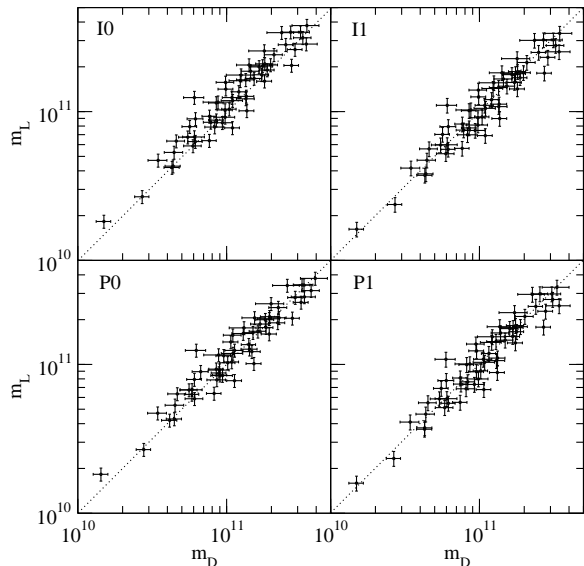


Fig. 2.— Dynamical and lensing estimates of the projected mass enclosed in the Einstein radius in units of solar mass. Plots are for the best fit of each model, designated at the superior left corner of each panel.

ever, the additional parameter of this model leads to just a modest improvement in reducing the mass discrepancy.

Finally, model P1 has two free parameters: the slope of the density profile and the mass contamination fraction. Figure 1 shows the likelihood contours in parameter space corresponding to several confidence levels. The best fit corresponds to a quasi-isothermal profile, $\gamma \simeq -2.1$, and a 13% contamination.

We have estimated the significance of evidence variations through the bootstrap technique. We have performed 300 bootstrap simulations of our lens sample and analyzed each of them with our four models. The distribution of evidence values obtained in the bootstrap simulation implies an uncertainty in values of $\Delta \ln E$ of approximately 0.9. Therefore our conclusions based on Bayes evidence comparison are statically robust.

The Bayesian evidence analysis (Table 1) indicates that there is a nominal gain in evidence when contamination is allowed. A 12.3 gain from model I0 to I1, and a 5.5 gain from model P0 to P1, both meaning strong evidence in favor of contamination, in terms of the qualitative Jeffreys scale (Trotta 2007). A comparison of models I0 with P0 and I1 with P1, shows that allowing a free power-law slope only gives a gain in evidence when there is no contamination. The gain in evidence from model I0 to P0 is 5.6, what means that there is moderate to strong evidence in favor of P0 in relation to I0. When contamination is taken into account, the added complexity of a free power-law profile slope does not pay the increment in likelihood. The evidence gain from model I1 to P1 is -1.2, what means that the Bayes analysis does not favors model P1 over I1.

It is worth mentioning at this point that we also examined the case of no seeing correction for all models and found the difference to be negligible. In fact, for models with SIS profile, $\sigma_p^2(\theta)$ is a constant, so the ratio present on Eq.(6) is one. There is no seeing correction in this particular case. The mean value of $\sigma_{ap}^2 / (\sigma_{ap}^2)_{obs}$ at the point of maximum likelihood in the parameter space is ≈ 1.002 for model P1, and even closer to unit for P0.

4. Discussion and Conclusion

Two independent methods, strong gravitational lensing and stellar dynamics, were used to determine the projected galaxy mass within its Einstein radius for a set of 58 galaxies from SLACS. From the comparison of the two masses, the lens density profile and l.o.s. mass contamination were probed.

We found that the lensing mass is overestimated in relation to the dynamical mass when the galaxy-lens is considered to be the only light deflecting potential. Interpreting this mass discrepancy as being due to secondary matter along the l.o.s., we obtained that models that take this contamination into account are strongly favored over models that do not, and that the effect is of the order of 10% on the lens mass. This result is in agreement with theoretical expectations coming from large-scale structure simulations (Premadi & Martel 2004; Hilbert et al. 2007; Faure et al. 2008; Puchwein & Hilbert 2009) and also with some observational works (Momcheva et al. 2006; Williams et al. 2006; Treu et al. 2008). A possible exception would be the the result of Auger (2008), who did not find an over-density of photometric sources along the l.o.s. of a sample of SLACS strong lenses in comparison with other SDSS massive early-type galaxies. However, it is worth pointing out that this is not in contradiction with the existence of mass over-densities along the l.o.s. since SLACS lenses were selected to be isolated and excess photometric sources would only trace rare high density peaks, but not more common diffuse mass concentrations.

The preferred total galactic density profile found in our analysis is compatible within 1σ with an isothermal. A similar result that was also obtained by other authors, apparently as a result of the complementarity of baryonic and dark matter profiles (Hamana et al. 2005; Ferreras et al. 2005; Lintott et al. 2006; Baltz et al. 2007; Czoske et al. 2008).

We used standard assumptions and approximations in our modeling of galaxies and analyzes. Nevertheless, we can identify several areas where further work can be done to refine the understanding of the effect of l.o.s. contamination on galaxy-scale strong lensing. Among them we highlight (i) the triaxiality and substructure of lens halos, whose importance was already suggested by

Meneghetti et al. (2005) and Yencho et al. (2006) in the context of simulations on cluster scales; (ii) the correction of the dynamical mass estimate due to rotational support. It is well known that some early-type galaxies can have a significant rotation component (e.g., Emsellem et al. 2007) and two-dimensional kinematics for some few SLACS lenses are already becoming available (Czoske et al. 2008; Barnabe et al. 2009); and (iii) the brightness distribution, which could be treated more realistically with the observed full surface luminosities for the individual lenses, instead of individualized fits of an universal profile.

The relaxation of some of our assumptions, with the addition of extra parameters, could prove a fruitful source of investigation, however would likely require a larger galaxy sample to reduce the increased degeneracies among the free parameters. Models with a large number of parameters may have a higher likelihood but lower Bayesian evidence, since the added complexity must pay its price in a Bayesian sense. In the case of the secondary matter along the l.o.s. we demonstrated that the added complexity is worth and should be taken into account in future studies of galaxy-scale strong lenses.

The authors thank CNPq and FAPESP for financial support and the SLACS and SDSS teams for the databases used in this work.

REFERENCES

- Auger, M. W. 2008, MNRAS, 383, L40
- Baltz, E. A., Marshall, P., & Oguri, M. 2007, ArXiv e-prints, arXiv:0705.0682
- Bar-Kana, R. 1996, ApJ, 468, 17
- Barnabè, M., & Koopmans, L. V. E. 2007, ApJ, 666, 726
- Barnabe, M., Czoske, O., Koopmans, L., Treu, T., Bolton, A., & Gavazzi, R. 2009, arXiv:0904.3861
- Binney, J. & Tremaine, S. 1987, Galactic Dynamics (Princeton: Princeton Univ. Press)
- Bolton, A. S., Burles, S., Koopmans, L. V. E., Treu, T., & Moustakas, L. A. 2006, ApJ, 638, 703
- Bolton, A. S., Burles, S., Treu, T., Koopmans, L. V. E., & Moustakas, L. A. 2007, ApJ, 665, L105
- Bolton, A. S., Burles, S., Koopmans, L. V. E., Treu, T., Gavazzi, R., Moustakas, L. A., Wayth, R., & Schlegel, D. J. 2008, ApJ, 682, 964
- Bolton, A. S., Treu, T., Koopmans, L. V. E., Gavazzi, R., Moustakas, L. A., Burles, S., Schlegel, D. J., & Wayth, R. 2008, ApJ, 684, 248
- Czoske, O., Barnabè, M., Koopmans, L. V. E., Treu, T., & Bolton, A. S. 2008, MNRAS, 384, 987
- Dalal, N., Hennawi, J. F., & Bode, P. 2005, ApJ, 622, 99
- Emsellem, E., et al. 2007, ArXiv Astrophysics e-prints, arXiv:astro-ph/0703531
- Faure, C., et al. 2008, arXiv:0810.4838, ApJin press
- Ferreras, I., Saha, P., & Williams, L. L. R. 2005, ApJ, 623, L5
- Gavazzi, R., Treu, T., Rhodes, J. D., Koopmans, L. V. E., Bolton, A. S., Burles, S., Massey, R. J., & Moustakas, L. A. 2007, ApJ, 667, 176
- Hamana, T., Ohyama, Y., Chiba, M., & Kashikawa, N. 2005, ArXiv Astrophysics e-prints, arXiv:astro-ph/0507056
- Hernquist, L. 1990, ApJ, 356, 359
- Hilbert, S., White, S. D. M., Hartlap, J., & Schneider, P. 2007, MNRAS, 927
- Keeton, C. R., Kochanek, C. S., & Seljak, U. 1997, ApJ, 482, 604
- Koopmans, L. V. E., Treu, T., Bolton, A. S., Burles, S., & Moustakas, L. A. 2006, ApJ, 649, 599
- Lintott, C. J., Ferreras, I., & Lahav, O. 2006, ApJ, 648, 826
- Meneghetti, M., Bartelmann, M., Jenkins, A., & Frenk, C. 2005, ArXiv Astrophysics e-prints, arXiv:astro-ph/0509323

- Meylan, G., Jetzer, P., North, P., Schneider, P., Kochanek, C. S., & Wambsganss, J. 2006, Saas-Fee Advanced Course 33: Gravitational Lensing: Strong, Weak and Micro
- Momcheva, I., Williams, K., Keeton, C., & Zabludoff, A. 2006, ApJ, 641, 169
- Moustakas, L. A., et al. 2007, ApJ, 660, L31
- Premadi, P., & Martel, H. 2004, ApJ, 611, 1
- Puchwein, E., & Hilbert, S. 2009, arXiv:0904.0253
- Treu, T., Koopmans, L. V., Bolton, A. S., Burles, S., & Moustakas, L. A. 2006, ApJ, 640, 662
- Treu, T., Gavazzi, R., Gorecki, A., Marshall, P. J., Koopmans, L. V. E., Bolton, A. S., Moustakas, L. A., & Burles, S. 2008, arXiv:0806.1056
- Trotta, R. 2007, MNRAS, 378, 72
- Yencho, B. M., Johnston, K. V., Bullock, J. S., & Rhode, K. L. 2006, ApJ, 643, 154
- Wambsganss, J., Bode, P., & Ostriker, J. P. 2005, ApJ, 635, L1
- Williams, K. A., Momcheva, I., Keeton, C. R., Zabludoff, A. I., & Lehár, J. 2006, ApJ, 646, 85